Microfluid Nanofluid (2010) 8:703–708
DOI 10.1007/s10404-009-0542-2

SHORT COMMUNICATION

Structure and charging kinetics of electrical double layers at large electrode voltages

Clint Cagle · Guang Feng · Rui Qiao · Jingsong Huang · Bobby G. Sumpter · Vincent Meunier

Received: 3 October 2009 / Accepted: 18 November 2009 / Published online: 18 December 2009

Abstract The structure and charging kinetics of electrical double layers (EDLs) at interfaces of NaCl solutions and planar electrodes are studied by molecular dynamics (MD) and Poisson–Nernst–Planck (PNP) simulations. Based on the MD results and prior experimental data, we show that counterion packing in planar EDLs does not reach the steric limit at electrode voltages below 1 V. In addition, we demonstrate that a PNP model, when complemented with a Stern model, can be effectively used to capture the overall charging kinetics. However, the PNP/Stern model can only give a qualitative description of the fine features of the EDL.

The structure and charging kinetics of the electrical double layers (EDLs) near polarized electrodes play a key role in many engineering systems, such as electrochemical capacitors (ECs) and AC electro-osmotic (AC-EO) pumps (Conway 1999; Ajdari 2000). The equilibrium EDL structure and the charging kinetics are typically modeled using the Poisson–Boltzmann (PB) equation and the Poisson–Nernst–Planck (PNP) equations (Conway 1999), respectively. It is established that the EDLs near electrodes with low voltages ($V < k_BT/e \approx 26$ mV at room temperature) and in dilute electrolytes can be described by these classical theories (Bazant et al. 2004). However, the EDLs near electrodes with large voltages ($V \gg k_BT/e$) and in concentrated electrolytes are much less understood, e.g., the ion concentration predicted by these models sometimes exceeds the steric limit (Kilic et al. 2007; Storey et al. 2008), and it is not clear whether the PNP model can accurately predict the charging kinetics. Whether the steric limit of ion packing is reached at large electrode voltages is important because such a phenomenon can help explain a long-standing puzzle in AC-EO pumping, namely the reversal of flow direction at high AC frequency and voltage (Storey et al. 2008; Studer et al. 2004). Since the PNP model is widely used to predict the charging kinetics in ECs and AC-EO pumps, it is also of great interest to delineate its accuracy. Atomistic simulations complement theoretical and experimental studies (Macdonald 1954; Macdonald and Barlow Jr 1967) because they can provide a detailed picture of the EDLs that is difficult to measure in experiments and also avoid some simplifications in theoretical models, e.g., the omission of the discreteness of solvent in describing EDLs. Prior atomistic simulations have provided insights on the EDL structure near the electrodes (Spohr 1999; Crozier et al. 2000), but important effects such as image forces were accounted for only in a few recent studies (Alawneh and Henderson 2007; Bhuiyan et al. 2007), and direct simulation of EDL charging has not been reported. In this study, we investigate EDLs at interfaces of a concentrated NaCl solution and planar electrodes under large voltages using molecular dynamics (MD) simulations and with the PNP model.

The MD simulations feature a pair of electrodes enclosing a slab of NaCl solution. Figure 1 shows a schematic of the MD system. The system is composed of 693 water molecules and 23 pairs of ions, and periodic boundary conditions are used in directions parallel to the electrodes. Simulation systems with similar sizes have been

C. Cagle · G. Feng · R. Qiao (✉)
College of Engineering and Science, Clemson University, Clemson, SC 29634-0921, USA
e-mail: rqiao@clemson.edu
URL: http://www.clemson.edu/~rqiao

J. Huang · B. G. Sumpter · V. Meunier
Oak Ridge National Laboratory, Bethel Valley Road, Oak Ridge, TN 37831-6367, USA

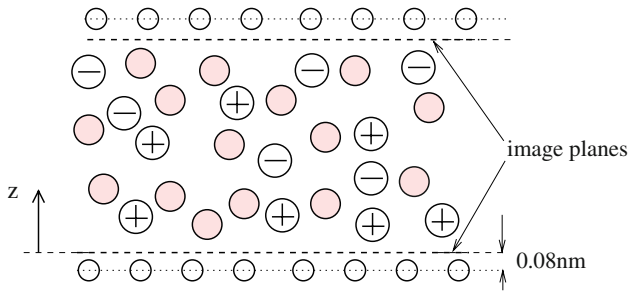

Fig. 1 A schematic of the MD simulation system. The empty circles denote the electrode atoms and the filled circiles denote water molecules

shown to be capable of predicting the ion mobility and hydration well (Lee and Rasaiah 1996). The ion concentration and pressure, measured at the center of the electrolyte slab under zero electrode potential, were equal to 2.0 M and 1.0 bar, respectively. Each electrode was modeled as a single layer of carbon atoms. Force fields for water and ions are taken from Smith and Dang (1994), and these force fields have been shown to reproduce the hydration and mobility of ions well (Lee and Rasaiah 1996). Constant electric potentials are enforced on each electrode using the method in Raghunathan and Aluru (2007). The image plane of each electrode was taken to be 0.08 nm from its geometric plane (Lang and Kohn 1971). The coordinate system was chosen such that the image plane of the lower electrode lies at $z = 0$. It is known that the distance between the effective image plane and the metal atom skeleton changes as the electrode charge density varies (Schmickler and Henderson 1986; Kornyshev 1989). Here, a fixed image plane is adopted to achieve a balance between simulation accuracy and computational cost. Specifically, using a fixed image plane already enables us to account for image forces neglected in most atomistic simulations with moderate computational cost. A more rigorous modeling that take into account the quantum nature of electrons in the electrode will require significantly more computational cost (the few existing simulations of such type are limited to equilibrium systems of very small sizes; Halley 1996). Since the charging kinetics depends most directly on the ion behavior in the electrolyte, the present approach should provide a reasonably accurate picture of the EDL charging kinetics. MD simulations were performed using a modified Gromacs package (Lindahl et al. 2001) in the NVT ensemble (T = 300 K). The slab-particle mesh Ewald (PME) method was used to compute the long-ranged electrostatic interactions (Yeh and Berkowitz 1999), and other MD details can be found in our earlier article (Qiao and Aluru 2003). Each system was first equilibrated under zero potential difference for 1.0 ns. At $t = 0$, a potential difference of 2 V was imposed between the electrodes, and simulation was run for 400 ps to study the charging kinetics. Since the electrodes are modeled as blocking electrodes, ideally a potential difference of less than 1.0–1.5 V (Bard and Faulkner 2001) should be used to investigate the EDL charging kinetics. Our simulations using such small potential difference (e.g., 0.5 and 1.0 V) produced similar results in charging kinetics, but the large statistical error prevents an accurate characterization of the charging kinetics. Hence, a potential difference of 2 V was used. In order to reduce the computational cost, the lateral span of the channel is 2.75 nm and a small separation between the image planes of the two electrodes (3.3 nm) was chosen here. As such, a strong electric field ($\sim O(1\text{V/nm})$) is generated inside the MD simulation system. Inside the EDL, this field is comparable to that in typical ECs (Conway 1999). Outside the EDL, the field decays quickly to zero as the EDL becomes charged. Since the response of electrolyte to these fields is in the linear regime (e.g., ion mobility remains constant), these electric fields do not introduce artifacts in the simulation of the charging kinetics. A total of 112 simulations with independent initial configurations were performed.

The EDLs in the above MD system were also studied using classical PNP models (Bazant et al. 2004; Franceschetti and Macdonald 1979) with the help of the COMSOL package (COMSOL 2005). A Stern layer model was used to complement the PNP model, i.e., the boundary condition for the electric potential ϕ on the lower ($z = 0$) and upper ($z = w$) electrode surfaces is given by Bazant et al. (2004)

$$\phi|_{z=0,w} = V_{\mp} \pm \lambda_s^{l,u} \mathrm{d}\phi/\mathrm{d}z|_{z=0,w}, \tag{1}$$

where $V_{\mp}$ are the potentials on the negative and positive electrodes, respectively. λ_s^l and λ_s^u are the effective thickness of the Stern layers near the lower and upper electrodes, respectively (Bazant et al. 2004). λ_s is related to the Stern layer thickness d_s by $\lambda_s = d_s\epsilon_b/\epsilon_s$, where ϵ_b and ϵ_s are the dielectric constants in the bulk and in the Stern layer, respectively. The key parameters of the PNP/Stern model include ion mobilities, separation between the two electrodes, and the effective Stern layer thickness λ_s^l and λ_s^u. In order to facilitate the comparison of the MD and PNP/Stern model predictions, the PNP/Stern model must be parameterized. Here, the ion mobilities ($\mu_{Na^+} = 2.11 \times 10^{-8}\,\mathrm{m^2/Vs}$ and $\mu_{Cl^-} = 3.37 \times 10^{-8}\,\mathrm{m^2/Vs}$) are taken from those computed from independent MD simulations. The dielectric constant of the bulk solution ε_b is taken as 78. Other parameters of the PNP/Stern model are discussed as follows.

We first examine the equilibrium structure of the EDLs when a potential difference of 2 V is enforced between the two electrodes. Figure 2a shows the ion concentrations between the electrodes. Near both electrodes, counterions can only approach the electrode to a finite distance and the

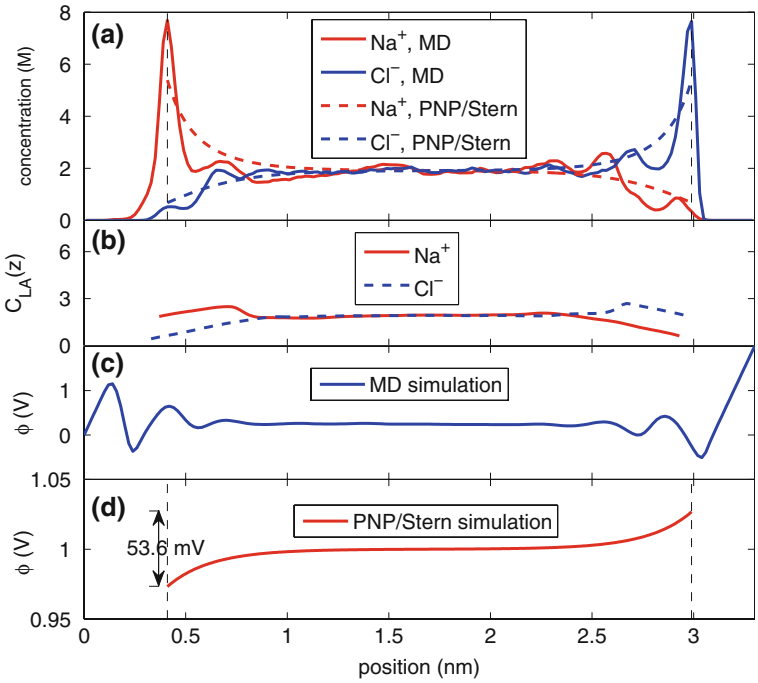

Fig. 2 Equilibrium ion concentrations and electric potentials between two blocking electrodes with a potential difference of 2 Volts. The space between the electrodes was divided into 165 bins in the z-direction to compute the ion concentration and electrical potential in MD simulations. (*a*) Na^+ and Cl^- ion concentration profiles obtained from MD and PNP/Stern simulations. The *dash lines* denote the position of electrode surface in the PNP/Stern simulations. (*b*) Locally averaged Na^+ and Cl^- concentrations defined in the text. (*c*) Potential distribution obtained from MD simulations. (*d*) Potential distribution obtained from PNP/Stern simulations

ion concentration profile shows local oscillations. The moderate distance ($\approx$0.4 nm) between the first counterion concentration peaks and the electrodes is caused by the finite size of the counterions (Qiao and Aluru 2003) and the fact that ions that approach very close to an electrode must shed part of their hydration shell (Qiao and Aluru 2005). Since the distance between the first counterion concentration peak and the electrode is comparable to the hydration radius of both the Na^+ and Cl^- ions, the ions located in these peaks are well-hydrated. Since the Debye length (0.21 nm) is much smaller than the channel width, an electro-neutral region is observed in the center of the channel. We define a locally averaged ion concentration $C_{\mathrm{LA}}(z,\, h)$ as the mean ion concentration in a bin (thickness: h) parallel to the electrode and centered at position z. The Steric limit is reached if $C_{\mathrm{LA}}\ (z, D_{\mathrm{hyd}})$ at any position z in the EDL approaches the close packing concentration C_{max} corresponding to the hydrated diameter of ions D_{hyd}. For Na^+ and Cl^- ions, whose hydrated diameters are 0.72 and 0.66 nm, respectively (Qiao and Aluru 2003), the corresponding close packing concentrations C_{max} are 6.29 and 8.17 M, respectively. Figure 2b shows $C_{\mathrm{LA}}(z, D_{\mathrm{hyd,Na^+}})$ and $C_{\mathrm{LA}}(z, D_{\mathrm{hyd,Na^+}})$, and we observe that both Na^+ and Cl^- ion concentrations are below the steric limit. In order to test the extent that ion distribution can be reproduced by the PNP/Stern model, we parameterize it using MD data. First, the electrode separation in the model is set to $w = 2.58$ nm, which is the distance between the first density peak of the Na^+ and the Cl^- ion near the negative and positive electrode. Next, we set $\lambda_s^l = \lambda_s^u = 7.65$ nm, so that the equilibrium electrode charge density σ_s obtained from the PNP/Stern model matches with that obtained from MD simulations ($\pm$ 0.087 C/m^2). In the systems studied, the Stern layer thickness d_s can be taken as 0.4 nm based on results shown in Fig. 2a. Therefore, a λ_s of 7.65 nm corresponds to a dielectric constant of 4.1 in the Stern layer, which is comparable to that reported in the literature (values of 6–20 are often reported; Conway 1999). The equilibrium ion concentration distributions obtained from the PNP/Stern model parameterized as above are shown in Fig. 2a along with the MD results. We observe that the PNP/Stern predictions did not fully capture the fine features of the ion distribution, e.g., the non-monotonic counter-ion concentration distribution predicted by MD simulations is not predicted by the PNP/Stern model. This is expected, since the PNP/Stern model is based on mean-field theory, and cannot effectively account for the ion hydration effects and the fluctuation potentials due to ion–ion correlation, which have been demonstrated to affect the ion distributions (Outhwaite and Bhuiyan 1982; Henderson and Boda 2009; Burak and Andelman 2000). However, given the simplicity of the PNP/Stern model used here, the overall agreement of the PNP/Stern prediction with the MD results is rather reasonable. It is important to note that the unphysically high counterion concentration that can arise in the standard PNP prediction (without the Stern layer model) for large electrode voltages is avoided in the present PNP/Stern model. This is because, when the Stern layer is accounted for, the electric potential drop across the diffuse EDL is reduced from 2 V to 53.6 mV (see Fig. 2d). These results suggest that a well-parameterized PNP/Stern model can predict the ion distribution in EDL semi-quantitatively.

However, because the molecular nature of water is not incorporated with sufficient accuracy into the PNP/Stern model, such a model cannot be used to study all EDL phenomena. For example, Fig. 2c shows the electric potential distribution between the two electrodes. The significant oscillation of electric potential near the electrode, caused by the discrete nature of ions and water molecules and predicted in earlier theoretical studies (Spohr 1999; Macdonald and Liu 1983), differs qualitatively from that obtained from the PNP/Stern model (see Fig. 2d). In addition, the potential distribution obtained from MD simulations shows significant asymmetry, e.g., the potential at the channel center is 0.25 V instead of the 1.0 V predicted by the PNP/Stern model. In order to understand this, we note that, in MD simulations, due to the strong orientation ordering of water near the electrode (Spohr 1999), there exists a potential drop of about 0.35 V between the electrode and the bulk electrolyte in the channel center when the electrode charge density is zero. Due to this, the potential drop between the positive electrode and the bulk electrolyte will differ from the potential drop between the negative electrode and the bulk electrolyte as the electrodes become electrified.

We next examine the charging kinetics of the EDLs when a potential difference of 2 V is suddenly imposed between the two opposing electrodes. The charging is quantified by a charging factor $C_f(t) = 1 - Q(t)/Q_\infty = \int_0^{w/2} \rho_e(z,t)\mathrm{d}z / \int_0^{w/2} \rho_e(z,\infty)\mathrm{d}z$, where ρ_e is the ionic space charge density and w is the electrode separation. Figure 3 shows the charging factor as a function of time. We observe that, at $t > 20$ ps and $C_f < 10\%$ (i.e., the EDLs are less than 90% charged), which are conditions most relevant to engineering practice, both the MD and the PNP/Stern models predict a linear charging kinetics

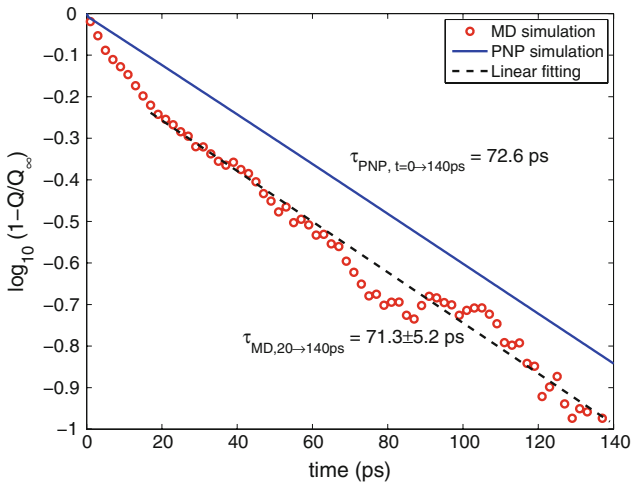

Fig. 3 Charging kinetics for the EDLs between two electrodes computed by using MD simulations and by using the PNP/Stern model. The voltage difference between the two electrodes is 2 Volts

(i.e., $C_f(t) \propto e^{-t/\tau}$). The time constant τ of the charging predicted by the PNP/Stern model (72.6 ps) agrees with that obtained from the MD simulation (71.3 ± 5.2 ps) within statistical error. At very short time ($t < 20$ ps), MD simulations predict a faster charging of the EDLs compared to the PNP/Stern model. In order to understand this, we note that, in the MD simulations, water cannot effectively screen the electric field emanating from the electrode at a time scale shorter than $O(10$ ps) due to the relatively slow molecular rotational motion, while water is assumed to respond instantaneously to any electric field in the PNP/Stern model. As such, at very short time after a potential difference is imposed between the two opposing electrodes, the electric field inside the electrolyte solution obtained by MD simulation is considerably stronger compared to that predicted by the PNP/Stern model, which subsequently leads to faster charging kinetics in the MD simulations. It is possible that the short time behavior of the charging kinetics might be captured more accurately if the frequency dependence of the dielectric behavior of water is accounted for in the PNP/Stern model, but this is beyond the scope of the present study.

A limitation of the present MD simulations is that the electronic degree of freedom of the electrode, which strongly affects the capacitance of the Stern (or Helmholtz) layer near metal surfaces (Conway 1999), was not accounted for. As such, the computed dependence of EDL structure on applied voltage should be regarded as semi-quantitative. However, since the liquid side of EDL is modeled in full detail, useful insights on dependence of EDL structure on the electrode charge density can still be obtained. Since the electrode charge density in the above simulations is below the maximum electrode charge density in typical aqueous electrolyte-based ECs, which falls in the range between −0.2 and 0.3 C/m^2 according to Conway (1999), we imposed charge densities of −0.26 and 0.26 C/m^2 on the negative and positive electrodes, which are close to the maximum charge densities in actual ECs, to explore the EDL structure (in particular, the ion packing) near electrodes. Figure 4 shows the equilibrium ion concentration profiles between the electrodes. It is observed that a layer of Na^+ ions adsorbs on the negative electrode and a second layer of Na^+ ion accumulates adjacent to the first Na^+ ion layer. As shown in our earlier studies, the second Na^+ ion layer originates from the ion hydration effect (Qiao and Aluru 2003; Qiao and Aluru 2005). Visualization of the MD system indicates that the Na^+ ions in the first layer approach closer to the electrode than the first interfacial water layer, which is not the case in Fig 2a. Since these ions are partly dehydrated, we cannot determine whether the steric limit is reached by computing the locally averaged ion concentration, whose definition involves the diameter of hydrated ions. However, the sharp

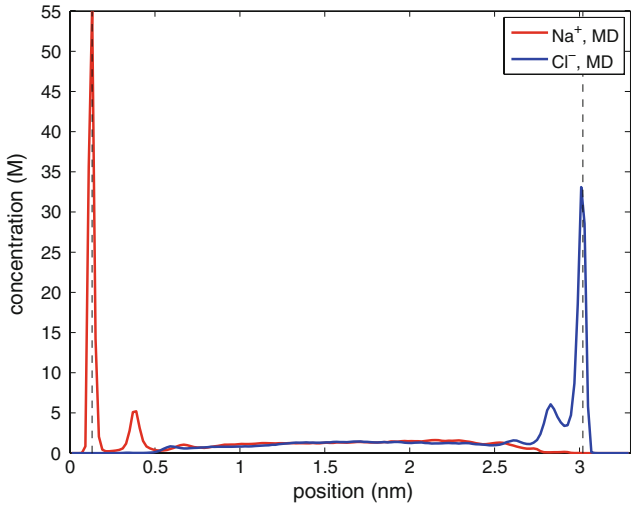

Fig. 4 Equilibrium ion concentration between two electrodes with charge densities of -0.26C/m^2 and 0.26C/m^2, respectively. The bin size used for computing the ion concentration is 0.02 nm

peak of the ion concentration profiles near both electrodes suggests that a compact layer forms near each electrode, and we can determine whether the steric limit is reached in this layer. Near the negative electrode, the compact layer occupies the space between the electrode and the first valley of the Na^+ ion concentration peak ($z = 0.23$ nm). Using the data in Fig. 4 and assuming that ions are hexagonally packed in this layer, the closest separation between these ions is found to be 0.92 nm. As this distance is larger than but comparable to the diameter of hydrated Na^+ ions (0.72 nm), we conclude packing of Na^+ ions are close to, but still below, the steric limit. Similarly, the closest separation between Cl^- ions in the compact layer near the positive electrode (taken as space between the electrode and the first Cl^- concentration valley) is 1.0 nm. Since this separation is larger than the diameter of hydrated Cl^- ions (0.66 nm), the packing of Cl^- ions is below the steric limit.

In summary, the above studies suggest that, despite the fact that the PNP/Stern model cannot capture the fine details of EDL structure and electric potential near electrodes (see Figs. 2c–d), a well-parameterized PNP/Stern model can still be used to predict the overall charging kinetics of EDLs under conditions relevant to typical engineering applications. The results in Fig. 4 suggest that the Na^+ ion packing near negative electrode is close to, but still below, the steric limit defined by the hydrated diameter of Na^+ ion at an electrode charge density of -0.26 C/m^2 and the Cl^- ion packing near positive electrode is below the steric limit at an electrode charge density of 0.26 C/m^2. Since the working voltage of ECs based on aqueous electrolytes is ≈ 1.0 V and the electrode charge density typically falls in the range of -0.2 C/m^2 to 0.3 C/m^2 in ECs (Conway 1999), we conclude that the packing of counterions near planar or mesoporous electrodes of such ECs does not reach the steric limit. Similarly, counterion packing are unlikely to reach the steric limit in AC-EO pumps working at voltages below 1.0 V. Hence, the decrease of differential capacitance of planar EDLs with increasing electrode potential in such a potential window is likely due to mechanisms other than steric packing of counterions (Schmickler and Henderson 1986). The steric limit of counterion packing in the EDL may be reached at even higher voltages and leads to a decrease of EDL capacitance as the electrode potential increases (Storey et al. 2008). However, under those conditions, significant Faradic reaction may occur and thus renders the physical picture much more complicated than that explored here. Simulation methods for studying the EDL charging under such conditions are currently under development.

Acknowledgments R.Q. thanks Professor Bazant at MIT for helpful discussions. The authors thank the Clemson-CCIT office for providing computer time. The Clemson authors acknowledge support from NSF under grant No. CBET-0756496. R.Q. was partly supported by an appointment to the HERE program for faculty at the Oak Ridge National Laboratory (ORNL) administered by ORISE. The authors at ORNL gratefully acknowledge the support from the Laboratory Directed Research and Development Program of ORNL and from U.S. Department of Energy under Contract No. DEAC05-00OR22725 with UT-Battelle, LLC at ORNL.

References

Ajdari A (2000) Pumping liquids using asymmetric electrode arrays. Phys Rev E 61:R45–R48

Alawneh M, Henderson D (2007) Monte Carlo simulation of the double layer at an electrode including the effect of a dielectric boundary. Mol Simulat 33:541–547

Bard AJ, Faulkner LR (2001) Electrochemical methods: fundamentals and applications, 2nd edn. Wiley, Hoboken, NJ

Bazant M, Thornton K, Ajdari A (2004) Diffuse-charge dynamics in electrochemical systems. Phys Rev E 70:021506

Bhuiyan LB, Outhwaite CW, Henderson D, Alawneh M (2007) Modified Poisson–Boltzmann theory and Monte Carlo simulation study of surface polarization effects in the planar diffuse double layer. Mol Phys 105:1395–1402

Burak Y, Andelman D (2000) Hydration interactions: Aqueous solvent effects in electric double layers. Phys Rev E 62:5296–5312

COMSOL (2005) Comsol multiphysics 3.2, chemical engineering module user guide. COMSOL AB, Burlington

Conway BE (1999) Electrochemical supercapacitors. Kluwer, New York

Crozier PS, Rowley RL, Henderson D (2000) Molecular dynamics calculations of the electrochemical properties of electrolyte systems between charged electrodes. J Chem Phys 113:9202–9209

Franceschetti DR, Macdonald JR (1979) Numerical analysis of electrical response: statics and dynamics of space-charge regions at blocking electrodes. J Appl Phys 50:291–302

Halley JW (1996) Studies of the interdependence of electronic and atomic dynamics and structure at the electrode–electrolyte interface. Electrochim Acta 41:2229–2251

Henderson D, Boda D (2009) Insights from theory and simulation on the electrical double layer. Phys Chem Chem Phys 11:3822–3830

Kilic MS, Bazant M, Ajdari A (2007) Steric effects in the dynamics of electrolytes at large applied voltages. I. Double-layer charging. Phys Rev E 75:021502

Kornyshev AA (1989) Metal electrons in the double layer theory. Electrochim Acta 34:1829–1847

Lang ND, Kohn W (1971) Theory of metal surfaces: work function. Phys Rev B 3:1215–1223

Lee SH, Rasaiah JC (1996) Molecular Dynamics Simulation of Ion Mobility. 2. Alkali Metal and Halide Ions Using the SPC/E Model for Water at 25°C. J Phys Chem 100:1420–1425

Lindahl E, Hess B, van der Spoel D (2001) GROMACS 3.0: a package for molecular simulation and trajectory analysis. J Mol Mod 7:306–317

Macdonald JR (1954) Theory of the differential capacitance of the double layer in unadsorbed electrolytes. J Chem Phys 22:1857–1866

Macdonald JR, Barlow CA Jr (1967) Theory of discreteness of charge effects in the electrolyte compact double layer. In: De Levie R (ed) Advances in electrochemistry and electrochemical engineering, Chap.1. Interscience, New York

Macdonald JR, Liu SH (1983) An iterated three-layer model of the double layer with permanent dipoles. Surf Sci 125:653–678

Outhwaite CW, Bhuiyan L (1982) A further treatment of the exclusion-volume term in the modified Poisson–Boltzmann theory of the electric double layer. J Chem Soc Faraday Trans 78:775–785

Qiao R, Aluru NR (2003) Ion concentrations and velocity profiles in nanochannel electroosmotic flows. J Chem Phys 118:4692–4701

Qiao R, Aluru NR (2005) Atomistic simulation of KCl transport in charged silicon nanochannels: interfacial effects. Colloids Surf A 267:103–109

Raghunathan AV, Aluru NR (2007) Self-consistent molecular dynamics formulation for electric-field-mediated electrolyte transport through nanochannels. Phys Rev E 76:011202

Schmickler W, Henderson D (1986) New models for the electrochemical interface. Prog Surf Sci 23:323–420

Smith DE, Dang LX (1994) Computer simulations of NaCl association in polarizable water. J Chem Phys 100:3757–3766

Spohr E (1999) Molecular simulation of the electrochemical double layer. Electrochim Acta 44:1697–1705

Storey BD, Edwards LR, Kilic MS, Bazant MZ (2008) Steric effects on ac electro-osmosis in dilute electrolytes. Phys Rev E 77:036317

Studer V, Pepin A, Chen Y, Ajdari A (2004) An integrated AC electrokinetic pump in a microfluidic loop for fast and tunable flow control. Analyst 129:944–949

Yeh I, Berkowitz M (1999) Ewald summation for systems with slab geometry. J Chem Phys 111:3155–3162